A Thick Anisotropic Plate Element in the Framework of an Absolute Nodal Coordinate Formulation

Cite as:
M. Langerholc, J. Slavič and M. Boltežar: A Thick Anisotropic Plate Element in the Framework of an Absolute Nodal Coordinate Formulation. Nonlinear Dynamics, 2013. DOI:10.1007/s11071-013-0778-y

Marko Langerholc[a,b], Janko Slavič[a], Miha Boltežar[a,]

[a] *University of Ljubljana, Faculty of Mechanical Engineering, Aškerčeva 6, 1000 Ljubljana, SI, Slovenia*
[b] *Knauf Insulation d.o.o., Trata 32, 4220 Škofja Loka, SI, Slovenia*

Abstract

In this research, the incorporation of material anisotropy is proposed for the large-deformation analyses of highly flexible dynamical systems. The anisotropic effects are studied in terms of a generalized elastic forces (GEFs) derivation for a continuum-based, thick and fully parameterized absolute nodal coordinate formulation plate element, of which the membrane and bending deformation effects are coupled. The GEFs are first derived for a fully anisotropic, linearly elastic material, characterized by 21 independent material parameters. Using the same approach, the GEFs are obtained for an orthotropic material, characterized by 9 material parameters. Furthermore, the analysis is extended to the case of nonlinear elasticity; the GEFs are introduced for a nonlinear Cauchy-elastic material, characterized by 4 in-plane orthotropic material parameters. Numerical simulations are performed to validate the theory for statics and dynamics to observe the anisotropic responses in terms of displacements, stresses and strains. The presented formulations are suitable for studying the nonlinear dynamical behaviour of advanced elastic materials of an arbitrary degree of anisotropy.

1. Introduction

Analyzing the nonlinear dynamical behaviour of complex engineering processes is becoming increasingly important, as the consideration of large deformations, the implementation of active external loadings, damping, friction or contact effects together with advanced, nonlinear, constitutive laws and material anisotropy, have in the past two decades put an emphasis on research in this field. Special large-deformation formulations were proposed to address the problems of nonlinear dynamics that allow the implementation of both the geometrical and material nonlinearities. Among the most recently proposed formulations is the absolute nodal coordinate formulation (ANCF).

The ANCF has been implemented in many different areas of mechanics, such as in characterization of highly nonlinear dynamical systems [29, 2, 9, 27], in studying contact problems [7, 11, 6], or even in the field of the digital image correlation [15]. Established especially to deal with highly flexible structures, the main features of the ANCF

are a constant mass matrix, zero centrifugal and Coriolis inertia forces and the possibility of exact rigid-body movement modelling. Since the ANCF is based on the general continuum theory, the assumptions of the classical beam and plate theories were systematically relaxed and more general finite elements were proposed [10, 1].

Among the element types, plate elements were also developed using 24, 36 or 48 nodal DOF. A thin-plate element formulation using 36 nodal DOF was investigated in [21, 28], where the formulation of the element's generalized elastic forces (GEFs) was based on the classic Kirchhoff theory. Furthermore, Mikkola and Shabana [18] presented a more general formulation of the plate with 48 nodal DOF, where the GEFs are obtained directly from the strain energy without its partitioning to the membrane and bending contribution. The latter (continuum) formulation includes the coupling between the membrane and bending effects and is therefore suitable for the analysis of thick and highly flexible systems, where the element's performance is not affected by the high-frequency deformation modes. Nevertheless, even though a variety of ANCF plates are developed, none of these formulations *a priori* considers the effects of material anisotropy.

When defining the material model of the analyzed continuum, the authors dealing with the ANCF managed to implement from basic, linearly elastic, to more advanced, nonlinear models. The latter include research done by Jung *et al.* and Maqueda and Shabana [17], who analyzed a rubber-like material, described by the Neo–Hookean and Mooney–Rivlin nonlinearly-elastic constitutive laws. Furthermore, Maqueda *et al.* [16] and Sugiyama *et al.* [25, 26] did extensive research on implementing elasto-plasticity. All these formulations incorporate advanced constitutive laws, yet the material is always assumed to be isotropic. In the ANCF, there seems to be a lack of research dealing with the effects of material anisotropy on the dynamic response of the analyzed systems. In many engineering processes, when dealing with laminated or composite plates, a consideration of anisotropy might be important. For example, just recently Nada and El-Assal [19] introduced a piezoelectric, laminated, thin ANCF plate plate as a *equivalent single layer* model. In addition, a real application dealing with a nonlinearly elastic and anisotropic material is the stone-wool production proces, where the nonlinear dynamics of the primary fleece during the folding process on the pendulum system is studied [14].

This research focuses on the effect of material anisotropy in the large-deformation analysis of highly flexible homogeneous elastic materials undergoing finite deformations. For the finite element, a thick, continuum-based, ANCF plate with 48 nodal DOF is studied, for which the GEFs are developed from the strain energy without its partitioning to the membrane and bending contribution. To address the effects of anisotropy, a procedure for the GEFs derivation is studied for a fully anisotropic (triclinic), linearly elastic material with 21 independent material parameters. Using the same procedure a lower-order anisotropic material is also studied. The procedure is further extended to the case of nonlinear elasticity; the GEFs for a nonlinear, orthotropic, Cauchy-elastic material are given. For this case, the tangent elastic properties are defined in a way to be able to characterize the dynamical behaviour using 4 independent material parameters.

Statical and dynamical numerical simulations are studied to validate the theory and show the anisotropic effects. The free-vibration response of a real orthotropic polyimide material is first studied in terms of the displacement and eigenfrequency analyses to assess the effects of the higher-frequency deformation modes. The second simulation deals with a static and dynamic analysis of a thick, nonlinearly elastic and orthotropic ANCF plate under a gravitational and external, time-dependent, vector-force loading. For the latter case, orientational material data is used to approach the real response of the aforementioned stone-wool fleece.

The paper is organized as follows: In Section 2, the ANCF thick plate formulation and the dynamic equations of

motion are summarized first. The derivation of the GEFs for the fully anisotropic material, the simplification for the orthotropic materials and the extension to the nonlinear case are shown in Section 3. The numerical simulations and results are presented in Section 4. The conclusions are given in Section 5.

2. Thick-plate dynamics

The thick ANCF plate element is a higher-order finite element [18], established in the framework of the general continuum theory with no *a priori* imposed simplifications or linearizations. An element of this kind is able to undergo finite rotation or deformation, it relaxes some of the assumptions used in the classic and Mindlin plate models [9] as well as automatically satisfies the objectivity requirements. Furthermore, the continuity of the displacement gradients between the nodal points of the element can be assured by using the appropriate shape functions. In the following, a short summary of the thick ANCF plate element is given in terms of the general formulation and the establishment of the equations of motion. For a detailed information the interested reader is referred to [18].

2.1. Thick ANCF plate formulation

The thick ANCF plate element possesses 48 nodal degrees of freedom (DOF). Even though designated as a plate, the element is treated as an isoparametric 3D solid body, for which the configuration is described in the Lagrangian formulation by [18]:

$$\mathbf{r}(\mathbf{x},\, t) = \mathbf{S}(\mathbf{x}) \cdot \mathbf{e}(t)\,, \tag{1}$$

where $\mathbf{x}$ is the initial position field in the local frame and $\mathbf{r}$ is the current position field in the global frame, respectively (Fig. 1):

$$\mathbf{x} = [x_1 \;\; x_2 \;\; x_3]^{\mathrm{T}}\,, \tag{2}$$

$$\mathbf{r} = [r_1 \;\; r_2 \;\; r_3]^{\mathrm{T}}\,, \tag{3}$$

and $\mathbf{S}$ is the global shape function matrix:

$$\mathbf{S} = \begin{bmatrix} S_1 & 0 & 0 & S_2 & 0 & 0 & & S_{16} & 0 & 0 \\ 0 & S_1 & 0 & 0 & S_2 & 0 & \cdots & 0 & S_{16} & 0 \\ 0 & 0 & S_1 & 0 & 0 & S_2 & & 0 & 0 & S_{16} \end{bmatrix}, \tag{4}$$

with S_i given in the Appendix. The influence of the element's thickness should be considered carefully; for a relatively thin element, oscillations of the gradients in the thickness direction $\mathbf{r}_{,x_3}$ may occur that lead to an increased numerical stiffness. Thin-plate formulations should be considered in that case, where the $\mathbf{r}_{,x_3}$ gradients and the corresponding shape functions S_k are eliminated from the formulation.

The vector $\mathbf{e}$ consists of the global nodal position coordinates and the nodal position-vector gradients:

$$\mathbf{e} = \left[\mathbf{e}^1 \;\; \mathbf{e}^2 \;\; \mathbf{e}^3 \;\; \mathbf{e}^4\right]^{\mathrm{T}}\,, \tag{5}$$

$$\mathbf{e}^i = \left[\mathbf{r}^{i\mathrm{T}} \;\; \left(\frac{\partial \mathbf{r}^i}{\partial x_1}\right)^{\mathrm{T}} \;\; \left(\frac{\partial \mathbf{r}^i}{\partial x_2}\right)^{\mathrm{T}} \;\; \left(\frac{\partial \mathbf{r}^i}{\partial x_3}\right)^{\mathrm{T}}\right], \quad i = 1, 2, 3, 4\,, \tag{6}$$

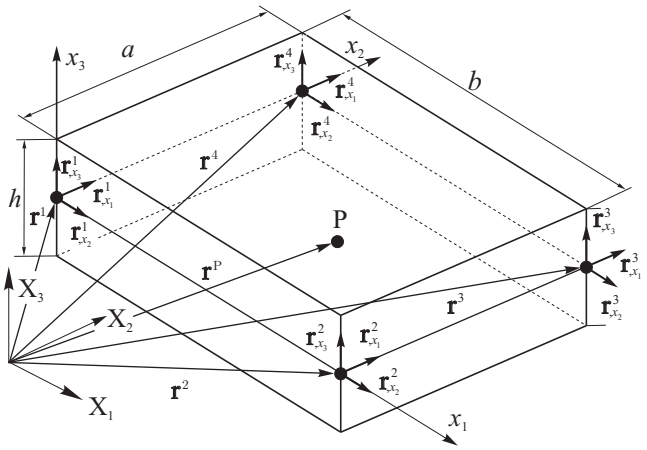

Figure 1: Parametrization of a thick ANCF plate element

which are used to define the matrix of the position-vector gradients:

$$\mathbf{J} = \frac{\partial \mathbf{r}}{\partial \mathbf{x}} = \begin{bmatrix} \mathbf{S}_{1,x_1} & \mathbf{S}_{1,x_2} & \mathbf{S}_{1,x_3} \\ \mathbf{S}_{2,x_1} & \mathbf{S}_{2,x_2} & \mathbf{S}_{2,x_3} \\ \mathbf{S}_{3,x_1} & \mathbf{S}_{3,x_2} & \mathbf{S}_{3,x_3} \end{bmatrix} \cdot \mathbf{e} \,, \tag{7}$$

where $\mathbf{S}_{i,x_k}$ is the differentiation of the i-th row of the matrix $\mathbf{S}$ with respect to the k-th initial coordinate in the element's local frame. In the ANCF, the nonlinear Green–Lagrange strain tensor is defined for the deformation measure [18], written in vector form as:

$$\boldsymbol{\varepsilon} = \frac{1}{2}\left[\mathbf{J}^{\mathrm{T}}\mathbf{J} - \mathbf{I}\right] \equiv [\varepsilon_{11} \;\; \varepsilon_{22} \;\; \varepsilon_{33} \;\; \varepsilon_{12} \;\; \varepsilon_{13} \;\; \varepsilon_{23}]^{\mathrm{T}} \,. \tag{8}$$

Note that the shear components in (8) are written as in [23], i. e., they are not multiplied by 2. Considering (1), the components ε_{ij} can be defined as:

$$\begin{aligned} \varepsilon_{11} &= \frac{1}{2}\left(\mathbf{e}^{\mathrm{T}}\mathbf{b}_1 \cdot \mathbf{e} - 1\right) \,, \quad \varepsilon_{22} = \frac{1}{2}\left(\mathbf{e}^{\mathrm{T}}\mathbf{b}_2 \cdot \mathbf{e} - 1\right) \,, \\ \varepsilon_{33} &= \frac{1}{2}\left(\mathbf{e}^{\mathrm{T}}\mathbf{b}_3 \cdot \mathbf{e} - 1\right) \,, \quad \varepsilon_{12} = \frac{1}{2}\,\mathbf{e}^{\mathrm{T}}\mathbf{b}_4 \cdot \mathbf{e} \,, \\ \varepsilon_{13} &= \frac{1}{2}\,\mathbf{e}^{\mathrm{T}}\mathbf{b}_5 \cdot \mathbf{e} \,, \quad \varepsilon_{23} = \frac{1}{2}\,\mathbf{e}^{\mathrm{T}}\mathbf{b}_6 \cdot \mathbf{e} \,, \end{aligned} \tag{9}$$

where:

$$
\begin{aligned}
\mathbf{b}_1 &= \mathbf{S}_{1,x_1} \otimes \mathbf{S}_{1,x_1} + \mathbf{S}_{2,x_1} \otimes \mathbf{S}_{2,x_1} + \mathbf{S}_{3,x_1} \otimes \mathbf{S}_{3,x_1} \,, \\
\mathbf{b}_2 &= \mathbf{S}_{1,x_2} \otimes \mathbf{S}_{1,x_2} + \mathbf{S}_{2,x_2} \otimes \mathbf{S}_{2,x_2} + \mathbf{S}_{3,x_2} \otimes \mathbf{S}_{3,x_2} \,, \\
\mathbf{b}_3 &= \mathbf{S}_{1,x_3} \otimes \mathbf{S}_{1,x_3} + \mathbf{S}_{2,x_3} \otimes \mathbf{S}_{2,x_3} + \mathbf{S}_{3,x_3} \otimes \mathbf{S}_{3,x_3} \,, \\
\mathbf{b}_4 &= \mathbf{S}_{1,x_1} \otimes \mathbf{S}_{1,x_2} + \mathbf{S}_{2,x_1} \otimes \mathbf{S}_{2,x_2} + \mathbf{S}_{3,x_1} \otimes \mathbf{S}_{3,x_2} \,, \\
\mathbf{b}_5 &= \mathbf{S}_{1,x_1} \otimes \mathbf{S}_{1,x_3} + \mathbf{S}_{2,x_1} \otimes \mathbf{S}_{2,x_3} + \mathbf{S}_{3,x_1} \otimes \mathbf{S}_{3,x_3} \,, \\
\mathbf{b}_6 &= \mathbf{S}_{1,x_2} \otimes \mathbf{S}_{1,x_3} + \mathbf{S}_{2,x_2} \otimes \mathbf{S}_{2,x_3} + \mathbf{S}_{3,x_2} \otimes \mathbf{S}_{3,x_3} \,,
\end{aligned}
\tag{10}
$$

with the outer product "⊗" of two vectors. It should be noted at this point that the matrices $\mathbf{b}_1$, $\mathbf{b}_2$ and $\mathbf{b}_3$ are symmetric, whereas $\mathbf{b}_4$, $\mathbf{b}_5$ and $\mathbf{b}_6$, are not. By differentiating the strain energy with respect to the vector of nodal coordinates, one obtains the vector of generalized elastic forces (GEFs) $\mathbf{Q}_\mathrm{e}$, written with Green–Lagrange strains [18]:

$$
\mathbf{Q}_\mathrm{e}(\mathbf{e}) = \frac{\partial}{\partial \mathbf{e}} \left(\frac{1}{2} \int_V \boldsymbol{\sigma}_{\mathrm{P2}} : \boldsymbol{\varepsilon} \, \mathrm{d}V \right) \,, \tag{11}
$$

where V is the reference volume and $\boldsymbol{\sigma}_{\mathrm{P2}}$ is the 2$^{\mathrm{nd}}$ Piola-Kirchhoff stress tensor.

2.2. Equations of motion

The continuum formulation of the thick ANCF plate, presented in Section 2.1, is incorporated into the formulation of the dynamic equations of motion. The background of the derivation of the equations of motion is well explained in many other publications, e.g. [22], and is only briefly summarized here to keep the paper focused.

In the ANCF, the absolute velocity vector $\dot{\mathbf{r}}$ is linear in nodal velocities $\dot{\mathbf{e}}$:

$$
\dot{\mathbf{r}} = \mathbf{S} \cdot \dot{\mathbf{e}} \,. \tag{12}
$$

The kinetic energy of the thick plate is therefore defined using (12):

$$
E_\mathrm{k} = \frac{1}{2} \int_V \rho \, \dot{\mathbf{r}}^\mathrm{T} \dot{\mathbf{r}} \, \mathrm{d}V = \frac{1}{2} \, \dot{\mathbf{e}}^\mathrm{T} \, \mathbf{M} \, \dot{\mathbf{e}} \,, \tag{13}
$$

where $\mathbf{M}$ is the constant mass matrix of the element:

$$
\mathbf{M} = \rho \int_V \mathbf{S}^\mathrm{T} \mathbf{S} \, \mathrm{d}V \,, \tag{14}
$$

with density ρ. Since the mass matrix is constant, the centrifugal and Coriolis inertia forces are equal to zero. Based on the principle of virtual work, this leads to a simplified form of the equations of motion [22]:

$$
\mathbf{M} \, \ddot{\mathbf{e}} = \mathbf{Q}_\mathrm{f} - \mathbf{Q}_\mathrm{e} \,, \tag{15}
$$

where $\mathbf{Q}_\mathrm{f}$ is the vector of the generalized external and damping nodal forces.

For our purpose, we will deal with both the external time-dependent force $\mathbf{Q}_{\mathrm{f,ex}}$ and the damping force $\mathbf{Q}_{\mathrm{f,d}}$. In the case of the time-dependent vector force $\mathbf{F}(t)$ at an arbitrary point "P" on the element (Fig. 1), the generalized nodal force is calculated as:

$$\mathbf{Q}_{\mathrm{f,ex}} = \mathbf{S}^{\mathrm{T}}(\mathbf{x}_{\mathrm{P}}) \cdot \mathbf{F} \, . \tag{16}$$

Further, the generalized damping force $\mathbf{Q}_{\mathrm{f,d}}$ is summarized according to [28]:

$$\mathbf{Q}_{\mathrm{f,d}} = \int_V \mathbf{S}^{\mathrm{T}} \cdot \mathbf{f}\,(\dot{\mathbf{r}}) \; \mathrm{d}V \, , \tag{17}$$

where $\mathbf{f}$ is the external, nonlinear damping force, representing, e.g., the air resistance:

$$\mathbf{f}\,(\dot{\mathbf{r}}) = \alpha_1 \, \dot{\mathbf{r}} + \alpha_2 \, \dot{\mathbf{r}} \; |\dot{\mathbf{r}}| \; , \tag{18}$$

with α_1 and α_2 as the parameters of the linear and quadratic damping term. By introducing (12) into (17), the generalized damping force is written as:

$$\mathbf{Q}_{\mathrm{f,d}} = \alpha_1 \int_V \mathbf{S}^{\mathrm{T}}\mathbf{S} \, \mathrm{d}V \cdot \dot{\mathbf{e}} + \alpha_2 \int_V \mathbf{S}^{\mathrm{T}}\mathbf{S} \, |\mathbf{S} \cdot \dot{\mathbf{e}}| \; \mathrm{d}V \cdot \dot{\mathbf{e}} \, . \tag{19}$$

When dealing with constraint dynamics, the algebraic kinematic constraint equations are introduced into (15). For our purpose, only the globally fixed joints and the time-independent joints between the two bodies will be considered. For the i-th body at the k-th node the fixed joint constraints are written as:

$$\mathbf{r}_i^k = \mathbf{S}(\mathbf{x}_i^k) \cdot \mathbf{e}_i = \mathbf{c}_i^k \, , \tag{20}$$

$$\frac{\partial \mathbf{r}_i^k}{\partial x_l} = \frac{\partial \mathbf{S}}{\partial x_l}(\mathbf{x}_i^k) \cdot \mathbf{e}_i = \mathbf{d}_{il}^k \, , \quad l = 1,2,3 \, , \tag{21}$$

where $\mathbf{c}_i^k$ and $\mathbf{d}_{il}^k$ are constant vectors. The joint between the i-th and j-th body at the k-th node is further formulated as:

$$\mathbf{S}(\mathbf{x}_i^k) \cdot \mathbf{e}_i = \mathbf{S}(\mathbf{x}_j^k) \cdot \mathbf{e}_j \, , \tag{22}$$

$$\frac{\partial \mathbf{S}}{\partial x_l}(\mathbf{x}_i^k) \cdot \mathbf{e}_i = \frac{\partial \mathbf{S}}{\partial x_l}(\mathbf{x}_j^k) \cdot \mathbf{e}_j \, , \quad l = 1,2,3 \, . \tag{23}$$

Based on Eqs. (20)-(23) a vector of constraint equations $\mathbf{C}$ is assembled [22] and differentiated with respect to the nodal variables to obtain the Jacobian matrix of kinematic constraints $\mathbf{C}_\mathbf{e} = \partial \mathbf{C} / \partial \mathbf{e}$. By employing the technique of Lagrange multipliers, the equations of motion for a constrained, flexible, multibody system can finally be expressed in a compact form as [22]:

$$\begin{bmatrix} \mathbf{M} & \mathbf{C}_\mathbf{e}^{\mathrm{T}} \\ \mathbf{C}_\mathbf{e} & \mathbf{0} \end{bmatrix} \begin{bmatrix} \ddot{\mathbf{e}} \\ \boldsymbol{\lambda} \end{bmatrix} = \begin{bmatrix} \mathbf{Q}_{\mathrm{e}} + \mathbf{Q}_{\mathrm{f}} \\ \mathbf{Q}_{\mathrm{d}} \end{bmatrix}, \tag{24}$$

where $\boldsymbol{\lambda}$ is the vector of Lagrange multipliers and $\mathbf{Q}_\mathrm{d}$ vector, which consists of the first and second time derivatives of the kinematic constraints. The Lagrange multipliers can be conveniently eliminated from (24), based on which the vector of nodal accelerations $\ddot{\mathbf{e}}$ can be derived as [13]:

$$\ddot{\mathbf{e}} = \mathbf{H}_{\mathbf{ee}} \cdot (\mathbf{Q}_\mathrm{e} + \mathbf{Q}_\mathrm{f}) + \mathbf{H}_{\mathbf{e}\boldsymbol{\lambda}} \cdot \mathbf{Q}_\mathrm{d} \,, \tag{25}$$

where:

$$\mathbf{H}_{\mathbf{ee}} = \mathbf{M}^{-1} - \mathbf{M}^{-1}\mathbf{C}_\mathbf{e}^\mathrm{T}\left(\mathbf{C}_\mathbf{e}\,\mathbf{M}^{-1}\mathbf{C}_\mathbf{e}^\mathrm{T}\right)^{-1}\mathbf{C}_\mathbf{e}\,\mathbf{M}^{-1} \,, \tag{26}$$

$$\mathbf{H}_{\mathbf{e}\boldsymbol{\lambda}} = \mathbf{M}^{-1}\mathbf{C}_\mathbf{e}^\mathrm{T}\left(\mathbf{C}_\mathbf{e}\,\mathbf{M}^{-1}\mathbf{C}_\mathbf{e}^\mathrm{T}\right)^{-1} \,. \tag{27}$$

Eq. (25) is finally integrated forward in time to obtain the velocities and coordinates ($\dot{\mathbf{e}}$, $\mathbf{e}$) [12]. It should be noted at this point that the Eqs. (26) and (27) require a calculation of the inverse matrix, which may, depending on the number of kinematic constraints, significantly affect the computational cost. However, in our case, the employed joints introduce kinematic constraints that are linear in terms of nodal variables. The Jacobian matrix $\mathbf{C}_\mathbf{e}$ is therefore constant, based on which the inverse matrices in (26) and (27) are calculated only once before the time integration.

The issue regarding the satisfaction of the kinematic constraints over time also needs to be mentioned. Since the kinematic constraints enter the equations of motion (24) in a differentiated form, the original constraints are violated to a degree that corresponds to the accuracy of the numerical integration. When using this approach, it is therefore necessary to examine the satisfaction of the constraints over the simulation time. If the accumulated errors are found to be unacceptable, coordinate partitioning techniques can be employed to circumvent this difficulty [22].

The presented computational procedure is general and suitable for analyses of dynamical systems regardless of the imposed material properties. We use it to study the dynamics of the thick ANCF plates with regard to the material anisotropy.

3. Generalized elastic forces for anisotropic materials

A procedure for the anisotropic GEFs (11) derivation is now presented. The GEFs depend on the element's nodal coordinates and hold all the information about the material of the continuum. Even in the case of linear elasticity, the GEFs are nonlinear in the nodal coordinates $\mathbf{e}$ and vary in complexity with regard to the number of independent material parameters in the elasticity matrix $\mathbf{E}$. To keep the procedure general, the derivation of the GEFs is shown for the case of a fully anisotropic material. The simplifications in terms of the number of independent elasticity matrix coefficients can be made later in order to obtain materials with a lower anisotropy order. In the following we presume that the principal material directions coincide with the local element's frame and the inertial frame, and therefore no transformation of material parameters is necessary.

In the case of fully anisotropic linear elasticity, the elasticity matrix $\mathbf{E}^\mathrm{A}$ is described by 21 independent coefficients

[20]:

$$\mathbf{E}^{\mathrm{A}} = \begin{bmatrix} c_{11} & c_{12} & c_{13} & c_{14} & c_{15} & c_{16} \\ c_{12} & c_{22} & c_{23} & c_{24} & c_{25} & c_{26} \\ c_{13} & c_{23} & c_{33} & c_{34} & c_{35} & c_{36} \\ c_{14} & c_{24} & c_{34} & c_{44} & c_{45} & c_{46} \\ c_{15} & c_{25} & c_{35} & c_{45} & c_{55} & c_{56} \\ c_{16} & c_{26} & c_{36} & c_{46} & c_{56} & c_{66} \end{bmatrix}, \tag{28}$$

and it is constant over the whole finite element. It should be noted here that the matrix $\mathbf{E}^{\mathrm{A}}$ does not depend on strain and is therefore constant even in the case of large deformations. This may not be an appropriate material law in some cases since the material may reach the limit of proportional elasticity, i. e., the tangent elastic properties may start to differ from the original elastic properties due to the effect of large deformations. However, for the sake of the simplicity of the following derivation it is presumed that the linear relation between the strain and the stress holds regardless of the amount of deformation.

The coefficients c_{ij} have a physical interpretation of being either uniaxial stiffnesses or generalized versions of the Poisson ratios, which measure the lateral contractions of a uniaxial tensile specimen. By using Eq. (28) to define the 2nd Piola–Kirchhoff stress vector:

$$\boldsymbol{\sigma}_{\mathrm{P2}} = \mathbf{E}^{\mathrm{A}} \cdot \boldsymbol{\varepsilon} \,, \tag{29}$$

the integral in (11) is written as a sum of 6 integrals:

$$\mathbf{Q}_{\mathbf{e}}^{\mathrm{A}} = \sum_{i=1}^{6} I_i^{\mathrm{A}} \,, \tag{30}$$

where, following the vector notation of (11):

$$\begin{aligned} I_1^{\mathrm{A}} &= \frac{1}{2} \int_V \frac{\partial}{\partial \mathbf{e}} \left(C_1 \cdot \varepsilon_{11} \right) \mathrm{d}V \,, \quad I_2^{\mathrm{A}} = \frac{1}{2} \int_V \frac{\partial}{\partial \mathbf{e}} \left(C_2 \cdot \varepsilon_{22} \right) \mathrm{d}V \,, \\ I_3^{\mathrm{A}} &= \frac{1}{2} \int_V \frac{\partial}{\partial \mathbf{e}} \left(C_3 \cdot \varepsilon_{33} \right) \mathrm{d}V \,, \quad I_4^{\mathrm{A}} = \frac{1}{2} \int_V \frac{\partial}{\partial \mathbf{e}} \left(C_4 \cdot \varepsilon_{23} \right) \mathrm{d}V \,, \\ I_5^{\mathrm{A}} &= \frac{1}{2} \int_V \frac{\partial}{\partial \mathbf{e}} \left(C_5 \cdot \varepsilon_{13} \right) \mathrm{d}V \,, \quad I_6^{\mathrm{A}} = \frac{1}{2} \int_V \frac{\partial}{\partial \mathbf{e}} \left(C_6 \cdot \varepsilon_{12} \right) \mathrm{d}V \,, \end{aligned} \tag{31}$$

with:

$$C_i = c_{i1}\, \varepsilon_{11} + c_{i2}\, \varepsilon_{22} + c_{i3}\, \varepsilon_{33} + c_{i4}\, \varepsilon_{23} + c_{i5}\, \varepsilon_{13} + c_{i6}\, \varepsilon_{12} \,, \quad i = 1, \ldots, 6 \,. \tag{32}$$

For different material groups, the variables C_i depend on the number of elastic constants in (28). To save space, the development of the integral I_1^{A} is shown here, only. The other integrals I_i^{A} are developed in the same way. First, we write I_1^{A} as a sum of 6 stiffness sub-integrals:

$$I_1^{\mathrm{A}} = \frac{1}{2} \int_V \frac{\partial}{\partial \mathbf{e}} \left(C_1 \cdot \varepsilon_{11} \right) \mathrm{d}V = \sum_{i=1}^{6} I_{1.i}^{\mathrm{A}} \,, \tag{33}$$

where:

$$
\begin{aligned}
I^{\mathrm{A}}_{1.1} &= \frac{c_{11}}{2}\int_V \frac{\partial}{\partial \mathbf{e}}\left(\varepsilon_{11}\,\varepsilon_{11}\right)\,\mathrm{d}V\,, \quad I^{\mathrm{A}}_{1.2} = \frac{c_{12}}{2}\int_V \frac{\partial}{\partial \mathbf{e}}\left(\varepsilon_{22}\,\varepsilon_{11}\right)\,\mathrm{d}V\,,\\
I^{\mathrm{A}}_{1.3} &= \frac{c_{13}}{2}\int_V \frac{\partial}{\partial \mathbf{e}}\left(\varepsilon_{33}\,\varepsilon_{11}\right)\,\mathrm{d}V\,, \quad I^{\mathrm{A}}_{1.4} = \frac{c_{14}}{2}\int_V \frac{\partial}{\partial \mathbf{e}}\left(\varepsilon_{23}\,\varepsilon_{11}\right)\,\mathrm{d}V\,,\\
I^{\mathrm{A}}_{1.5} &= \frac{c_{15}}{2}\int_V \frac{\partial}{\partial \mathbf{e}}\left(\varepsilon_{13}\,\varepsilon_{11}\right)\,\mathrm{d}V\,, \quad I^{\mathrm{A}}_{1.6} = \frac{c_{16}}{2}\int_V \frac{\partial}{\partial \mathbf{e}}\left(\varepsilon_{12}\,\varepsilon_{11}\right)\,\mathrm{d}V\,,
\end{aligned}
\tag{34}
$$

and analyze them individually. By considering the relations (9) and (10), integral $I^{\mathrm{A}}_{1.1}$ is equal to:

$$
\begin{aligned}
I^{\mathrm{A}}_{1.1} &= \frac{c_{11}}{8}\int_V \frac{\partial}{\partial \mathbf{e}}\left[\left(\mathbf{e}^{\mathrm{T}}\,\mathbf{b}_1\cdot\mathbf{e}\right)\left(\mathbf{e}^{\mathrm{T}}\,\mathbf{b}_1\cdot\mathbf{e}\right) - 2\left(\mathbf{e}^{\mathrm{T}}\,\mathbf{b}_1\cdot\mathbf{e}\right) + 1\right]\,\mathrm{d}V =\\
&= I^{\mathrm{A}}_{1.1\mathrm{a}} + I^{\mathrm{A}}_{1.1\mathrm{b}}\,,
\end{aligned}
\tag{35}
$$

where:

$$
\begin{aligned}
I^{\mathrm{A}}_{1.1\mathrm{a}} &= \frac{c_{11}}{8}\int_V \frac{\partial}{\partial \mathbf{e}}\left[\left(\mathbf{e}^{\mathrm{T}}\,\mathbf{b}_1\cdot\mathbf{e}\right)\left(\mathbf{e}^{\mathrm{T}}\,\mathbf{b}_1\cdot\mathbf{e}\right)\right]\,\mathrm{d}V\,,\\
I^{\mathrm{A}}_{1.1\mathrm{b}} &= -\frac{c_{11}}{8}\int_V \frac{\partial}{\partial \mathbf{e}}\left(\mathbf{e}^{\mathrm{T}}\,\mathbf{b}_1\cdot\mathbf{e}\right)\,\mathrm{d}V\,.
\end{aligned}
\tag{36}
$$

Using the relation [4]:

$$
\frac{\partial}{\partial \mathbf{e}}\left(\mathbf{e}^{\mathrm{T}}\,\mathbf{b}_i\cdot\mathbf{e}\right) = \mathbf{e}^{\mathrm{T}}\left(\mathbf{b}_i^{\mathrm{T}} + \mathbf{b}_i\right)\,,
\tag{37}
$$

the differentiation with respect to $\mathbf{e}$ is:

$$
\begin{aligned}
&\frac{\partial}{\partial \mathbf{e}}\left[\left(\mathbf{e}^{\mathrm{T}}\,\mathbf{b}_i\cdot\mathbf{e}\right)\left(\mathbf{e}^{\mathrm{T}}\,\mathbf{b}_j\cdot\mathbf{e}\right)\right] =\\
&\left(\frac{\partial}{\partial \mathbf{e}}\left(\mathbf{e}^{\mathrm{T}}\,\mathbf{b}_i\cdot\mathbf{e}\right)\right)\left(\mathbf{e}^{\mathrm{T}}\,\mathbf{b}_j\cdot\mathbf{e}\right) + \left(\mathbf{e}^{\mathrm{T}}\,\mathbf{b}_i\cdot\mathbf{e}\right)\left(\frac{\partial}{\partial \mathbf{e}}\left(\mathbf{e}^{\mathrm{T}}\,\mathbf{b}_j\cdot\mathbf{e}\right)\right) =\\
&= \left(\mathbf{e}^{\mathrm{T}}\left(\mathbf{b}_i^{\mathrm{T}} + \mathbf{b}_i\right)\right)\left(\mathbf{e}^{\mathrm{T}}\,\mathbf{b}_j\cdot\mathbf{e}\right) + \left(\mathbf{e}^{\mathrm{T}}\,\mathbf{b}_i\cdot\mathbf{e}\right)\left(\mathbf{e}^{\mathrm{T}}\left(\mathbf{b}_j^{\mathrm{T}} + \mathbf{b}_j\right)\right)\,.
\end{aligned}
\tag{38}
$$

Considering also $\mathbf{e}^{\mathrm{T}}\,\mathbf{b}_i = (\mathbf{b}_i\cdot\mathbf{e})^{\mathrm{T}} = \mathbf{b}_i^{\mathrm{T}}\cdot\mathbf{e}$ [4], and the fact that the matrices $\mathbf{b}_i$ for $i = 1, 2, 3$ are symmetric, Eq. (38) is written, factoring out $\mathbf{e}$:

$$
\frac{\partial}{\partial \mathbf{e}}\left[\left(\mathbf{e}^{\mathrm{T}}\,\mathbf{b}_i\cdot\mathbf{e}\right)\left(\mathbf{e}^{\mathrm{T}}\,\mathbf{b}_j\cdot\mathbf{e}\right)\right] = 2\left[\mathbf{b}_i^{\mathrm{T}}\left(\mathbf{e}^{\mathrm{T}}\,\mathbf{b}_j\cdot\mathbf{e}\right) + \left(\mathbf{e}^{\mathrm{T}}\,\mathbf{b}_j\cdot\mathbf{e}\right)\mathbf{b}_i\right]\cdot\mathbf{e}\,,
\tag{39}
$$

thus:

$$
\begin{aligned}
I^{\mathrm{A}}_{1.1\mathrm{a}} &= \frac{c_{11}}{4}\int_V \left[\mathbf{b}_1^{\mathrm{T}}\left(\mathbf{e}^{\mathrm{T}}\,\mathbf{b}_1\cdot\mathbf{e}\right) + \left(\mathbf{e}^{\mathrm{T}}\,\mathbf{b}_1\cdot\mathbf{e}\right)\mathbf{b}_1\right]\cdot\mathbf{e}\,\mathrm{d}V\,,\\
I^{\mathrm{A}}_{1.1\mathrm{b}} &= -\frac{c_{11}}{4}\int_V \mathbf{b}_1^{\mathrm{T}}\cdot\mathbf{e}\,\mathrm{d}V\,,
\end{aligned}
\tag{40}
$$

so the integral (35) takes the final form:

$$I_{1.1}^{\mathrm{A}} = \frac{c_{11}}{4} \int_V \left[\mathbf{b}_1^{\mathrm{T}} \left(\mathbf{e}^{\mathrm{T}} \mathbf{b}_1 \cdot \mathbf{e} - 1 \right) + \left(\mathbf{e}^{\mathrm{T}} \mathbf{b}_1 \cdot \mathbf{e} \right) \mathbf{b}_1 \right] \cdot \mathbf{e} \, \mathrm{d}V \, . \tag{41}$$

Similar to (35), we write the integral $I_{1.2}^{\mathrm{A}}$:

$$\begin{aligned} I_{1.2}^{\mathrm{A}} &= \frac{c_{12}}{8} \int_V \frac{\partial}{\partial \mathbf{e}} \left[\left(\mathbf{e}^{\mathrm{T}} \mathbf{b}_2 \cdot \mathbf{e} \right) \left(\mathbf{e}^{\mathrm{T}} \mathbf{b}_1 \cdot \mathbf{e} \right) - \left(\mathbf{e}^{\mathrm{T}} \mathbf{b}_2 \cdot \mathbf{e} \right) - \left(\mathbf{e}^{\mathrm{T}} \mathbf{b}_1 \cdot \mathbf{e} \right) + 1 \right] \mathrm{d}V = \\ &= I_{1.2\mathrm{a}}^{\mathrm{A}} + I_{1.2\mathrm{b}}^{\mathrm{A}} + I_{1.2\mathrm{c}}^{\mathrm{A}} \, , \end{aligned} \tag{42}$$

where:

$$\begin{aligned} I_{1.2\mathrm{a}}^{\mathrm{A}} &= \frac{c_{12}}{8} \int_V \frac{\partial}{\partial \mathbf{e}} \left[\left(\mathbf{e}^{\mathrm{T}} \mathbf{b}_2 \cdot \mathbf{e} \right) \left(\mathbf{e}^{\mathrm{T}} \mathbf{b}_1 \cdot \mathbf{e} \right) \right] \mathrm{d}V \, , \\ I_{1.2\mathrm{b}}^{\mathrm{A}} &= -\frac{c_{12}}{8} \int_V \frac{\partial}{\partial \mathbf{e}} \left(\mathbf{e}^{\mathrm{T}} \mathbf{b}_2 \cdot \mathbf{e} \right) \mathrm{d}V \, , \\ I_{1.2\mathrm{c}}^{\mathrm{A}} &= -\frac{c_{12}}{8} \int_V \frac{\partial}{\partial \mathbf{e}} \left(\mathbf{e}^{\mathrm{T}} \mathbf{b}_1 \cdot \mathbf{e} \right) \mathrm{d}V \, , \end{aligned} \tag{43}$$

which after some manipulation leads to the final form of $I_{1.2}^{\mathrm{A}}$:

$$I_{1.2}^{\mathrm{A}} = \frac{c_{12}}{4} \int_V \left[\mathbf{b}_2^{\mathrm{T}} \left(\mathbf{e}^{\mathrm{T}} \mathbf{b}_1 \cdot \mathbf{e} - 1 \right) + \left(\mathbf{e}^{\mathrm{T}} \mathbf{b}_2 \cdot \mathbf{e} - 1 \right) \mathbf{b}_1 \right] \cdot \mathbf{e} \, \mathrm{d}V \, . \tag{44}$$

In the same way as for (35) and (42), we write the integral $I_{1.3}^{\mathrm{A}}$:

$$I_{1.3}^{\mathrm{A}} = \frac{c_{13}}{4} \int_V \left[\mathbf{b}_3^{\mathrm{T}} \left(\mathbf{e}^{\mathrm{T}} \mathbf{b}_1 \cdot \mathbf{e} - 1 \right) + \left(\mathbf{e}^{\mathrm{T}} \mathbf{b}_3 \cdot \mathbf{e} - 1 \right) \mathbf{b}_1 \right] \cdot \mathbf{e} \, \mathrm{d}V \, . \tag{45}$$

The development of the integrals $I_{1.4}^{\mathrm{A}} - I_{1.6}^{\mathrm{A}}$ follows the same procedure as above, the derivations are only modified on account of the asymmetry of the matrices $\mathbf{b}_i$ for $i = 4, 5, 6$. For the sake of brevity, only the final forms are stated here; for $k = 4, 5, 6$, we have:

$$I_{1.k}^{\mathrm{A}} = \frac{c_{1k}}{8} \int_V \left[\left(\mathbf{b}_{10-k} + \mathbf{b}_{10-k}^{\mathrm{T}} \right) \left(\mathbf{e}^{\mathrm{T}} \mathbf{b}_1 \cdot \mathbf{e} - 1 \right) + 2 \left(\mathbf{e}^{\mathrm{T}} \mathbf{b}_{10-k} \cdot \mathbf{e} \right) \mathbf{b}_1 \right] \cdot \mathbf{e} \, \mathrm{d}V \, . \tag{46}$$

The integrals $I_{1.1}^{\mathrm{A}} - I_{1.6}^{\mathrm{A}}$ are finally summed together to form the stiffness integral (33):

$$\begin{aligned} I_1^{\mathrm{A}} = & \frac{1}{4} \int_V \left[\left(\sum_{i=1}^{3} c_{1i} \, \mathbf{b}_i^{\mathrm{T}} + \sum_{i=4}^{6} c_{1i} \left(\mathbf{b}_{10-i} + \mathbf{b}_{10-i}^{\mathrm{T}} \right) \right) \left(\mathbf{e}^{\mathrm{T}} \mathbf{b}_1 \cdot \mathbf{e} - 1 \right) + \right. \\ & \left. + \left(\sum_{i=1}^{3} c_{1i} \left(\mathbf{e}^{\mathrm{T}} \mathbf{b}_i \cdot \mathbf{e} \right) + \sum_{i=4}^{6} c_{1i} \left(\mathbf{e}^{\mathrm{T}} \mathbf{b}_{10-i} \cdot \mathbf{e} \right) - c_{12} - c_{13} \right) \mathbf{b}_1 \right] \cdot \mathbf{e} \, \mathrm{d}V \, . \end{aligned} \tag{47}$$

The derivation of the stiffness integrals $I_2^{\mathrm{A}} - I_6^{\mathrm{A}}$ is analogous, as shown above. We write:

$$I_k^{\mathrm{A}} = \sum_{i=1}^{6} I_{k.i}^{\mathrm{A}} \,, \quad k = 2, \ldots, 6 \,, \tag{48}$$

where the I_k^{A} for $k = 2, 3$ are, considering $c_{ij} = c_{ji}$:

$$\begin{aligned} I_k^{\mathrm{A}} =& \frac{1}{4} \int_V \left[\left(\sum_{i=1}^{3} c_{ki}\, \mathbf{b}_i^{\mathrm{T}} + \sum_{i=4}^{6} c_{ki} \left(\mathbf{b}_{10-i} + \mathbf{b}_{10-i}^{\mathrm{T}} \right) \right) \left(\mathbf{e}^{\mathrm{T}}\, \mathbf{b}_k \cdot \mathbf{e} - 1 \right) + \right. \\ &+ \left. \left(\sum_{i=1}^{3} c_{ki} \left(\mathbf{e}^{\mathrm{T}} \mathbf{b}_i \cdot \mathbf{e} \right) + \sum_{i=4}^{6} c_{ki} \left(\mathbf{e}^{\mathrm{T}} \mathbf{b}_{10-i} \cdot \mathbf{e} \right) - c_{k1} - c_{k3} \right) \mathbf{b}_k \right] \cdot \mathbf{e}\, \mathrm{d}V \,, \end{aligned} \tag{49}$$

and for $k = 4, 5, 6$:

$$\begin{aligned} I_k^{\mathrm{A}} =& \frac{1}{4} \int_V \left[\left(\sum_{i=1}^{3} 2\, c_{ki}\, \mathbf{b}_i^{\mathrm{T}} + \sum_{i=4}^{6} 2\, c_{ki} \left(\mathbf{b}_{10-i} + \mathbf{b}_{10-i}^{\mathrm{T}} \right) \right) \left(\mathbf{e}^{\mathrm{T}}\, \mathbf{b}_{10-k} \cdot \mathbf{e} \right) + \right. \\ &+ \left(\sum_{i=1}^{3} c_{ki} \left(\mathbf{e}^{\mathrm{T}} \mathbf{b}_i \cdot \mathbf{e} \right) + \sum_{i=4}^{6} c_{ki} \left(\mathbf{e}^{\mathrm{T}} \mathbf{b}_{10-k} \cdot \mathbf{e} \right) \right) \left(\mathbf{b}_{10-k} + \mathbf{b}_{10-i}^{\mathrm{T}} \right) - \\ &- \left. \mathbf{b}_{10-k}^{\mathrm{T}} \sum_{i=1}^{3} c_{ki} \right] \cdot \mathbf{e}\, \mathrm{d}V \,. \end{aligned} \tag{50}$$

The vector of the anisotropic GEFs (30) is equal to the sum of stiffness integrals (47)-(50).

If the analyzed material contains additional symmetries, the described procedure is simplified on account of there being fewer coefficients c_{ij}. In the following, two special cases of the GEFs of a lower-order anisotropy material are presented: the first is for a linearly elastic orthotropic material with 9 independent parameters, and the second for a nonlinearly elastic orthotropic material with 4 independent parameters.

3.1. Linearly elastic orthotropic material

Among engineering materials, composites frequently possess mutually perpendicular symmetry planes, i.e., they express orthotropic behaviour. Shear strains are not present by their uniaxial deformation, since the elasticity matrix (28), with superscript "O" denoting orthotropy, takes the form [20]:

$$\mathbf{E}^{\mathrm{o}} = \begin{bmatrix} c_{11}^{\mathrm{o}} & c_{12}^{\mathrm{o}} & c_{13}^{\mathrm{o}} & 0 & 0 & 0 \\ c_{12}^{\mathrm{o}} & c_{22}^{\mathrm{o}} & c_{23}^{\mathrm{o}} & 0 & 0 & 0 \\ c_{13}^{\mathrm{o}} & c_{23}^{\mathrm{o}} & c_{33}^{\mathrm{o}} & 0 & 0 & 0 \\ 0 & 0 & 0 & c_{44}^{\mathrm{o}} & 0 & 0 \\ 0 & 0 & 0 & 0 & c_{55}^{\mathrm{o}} & 0 \\ 0 & 0 & 0 & 0 & 0 & c_{66}^{\mathrm{o}} \end{bmatrix} , \tag{51}$$

where 9 independent coefficients are (using the Young moduli E_i and the Poisson ratios ν_{ij}):

$$\begin{aligned}
c^{\mathrm{o}}_{11} &= E_1\,(1-\nu_{23}\,\nu_{32})\,\gamma_{\mathrm{o}}\,, \quad c^{\mathrm{o}}_{44} = E_1/\,(1-\nu_{12})\,,\\
c^{\mathrm{o}}_{22} &= E_2\,(1-\nu_{13}\,\nu_{31})\,\gamma_{\mathrm{o}}\,, \quad c^{\mathrm{o}}_{55} = E_2/\,(1-\nu_{13})\,,\\
c^{\mathrm{o}}_{33} &= E_3\,(1-\nu_{21}\,\nu_{12})\,\gamma_{\mathrm{o}}\,, \quad c^{\mathrm{o}}_{66} = E_3/\,(1-\nu_{23})\,,\\
c^{\mathrm{o}}_{12} &= c^{\mathrm{o}}_{21} = E_1\,(\nu_{21}+\nu_{31}\,\nu_{23})\,\gamma_{\mathrm{o}} = E_2\,(\nu_{12}+\nu_{32}\,\nu_{12})\,\gamma_{\mathrm{o}}\,,\\
c^{\mathrm{o}}_{13} &= c^{\mathrm{o}}_{31} = E_1\,(\nu_{31}+\nu_{21}\,\nu_{32})\,\gamma_{\mathrm{o}} = E_3\,(\nu_{13}+\nu_{12}\,\nu_{23})\,\gamma_{\mathrm{o}}\,,\\
c^{\mathrm{o}}_{23} &= c^{\mathrm{o}}_{32} = E_2\,(\nu_{32}+\nu_{12}\,\nu_{31})\,\gamma_{\mathrm{o}} = E_3\,(\nu_{23}+\nu_{21}\,\nu_{13})\,\gamma_{\mathrm{o}}\,,
\end{aligned} \tag{52}$$

with:

$$\gamma_{\mathrm{o}} = \frac{1}{1-\nu_{12}\,\nu_{21}-\nu_{23}\,\nu_{32}-\nu_{31}\,\nu_{13}-2\,\nu_{21}\,\nu_{32}\,\nu_{13}}\,. \tag{53}$$

By following the same procedure as in Section 3, the orthotropic stiffness integrals (31) take the form:

$$\begin{aligned}
I^{\mathrm{o}}_1 =& \frac{1}{4}\int_V \Big[2\,c^{\mathrm{o}}_{11}\,\mathbf{b}_1^{\mathrm{T}}\left(\mathbf{e}^{\mathrm{T}}\,\mathbf{b}_1\cdot\mathbf{e}-1\right)+c^{\mathrm{o}}_{12}\left(\mathbf{b}_2^{\mathrm{T}}\left(\mathbf{e}^{\mathrm{T}}\,\mathbf{b}_1\cdot\mathbf{e}-1\right)+\left(\mathbf{e}^{\mathrm{T}}\,\mathbf{b}_2\cdot\mathbf{e}-1\right)\mathbf{b}_1\right)+\\
&+c^{\mathrm{o}}_{13}\left(\mathbf{b}_3^{\mathrm{T}}\left(\mathbf{e}^{\mathrm{T}}\,\mathbf{b}_1\cdot\mathbf{e}-1\right)+\left(\mathbf{e}^{\mathrm{T}}\,\mathbf{b}_3\cdot\mathbf{e}-1\right)\mathbf{b}_1\right)\Big]\cdot\mathbf{e}\,\mathrm{d}V\,.\\
I^{\mathrm{o}}_2 =& \frac{1}{4}\int_V \Big[c^{\mathrm{o}}_{12}\left(\mathbf{b}_1^{\mathrm{T}}\left(\mathbf{e}^{\mathrm{T}}\,\mathbf{b}_2\cdot\mathbf{e}-1\right)+\left(\mathbf{e}^{\mathrm{T}}\,\mathbf{b}_1\cdot\mathbf{e}-1\right)\mathbf{b}_2\right)+c^{\mathrm{o}}_{23}\left(\mathbf{b}_3^{\mathrm{T}}\left(\mathbf{e}^{\mathrm{T}}\,\mathbf{b}_2\cdot\mathbf{e}-1\right)+\right.\\
&\left.+\left(\mathbf{e}^{\mathrm{T}}\,\mathbf{b}_3\cdot\mathbf{e}-1\right)\mathbf{b}_2\right)+2\,c^{\mathrm{o}}_{22}\,\mathbf{b}_2^{\mathrm{T}}\left(\mathbf{e}^{\mathrm{T}}\,\mathbf{b}_2\cdot\mathbf{e}-1\right)\Big]\cdot\mathbf{e}\,\mathrm{d}V\,.\\
I^{\mathrm{o}}_3 =& \frac{1}{4}\int_V \Big[c^{\mathrm{o}}_{13}\left(\mathbf{b}_1^{\mathrm{T}}\left(\mathbf{e}^{\mathrm{T}}\,\mathbf{b}_3\cdot\mathbf{e}-1\right)+\left(\mathbf{e}^{\mathrm{T}}\,\mathbf{b}_1\cdot\mathbf{e}-1\right)\mathbf{b}_3\right)+c^{\mathrm{o}}_{23}\left(\mathbf{b}_2^{\mathrm{T}}\left(\mathbf{e}^{\mathrm{T}}\,\mathbf{b}_3\cdot\mathbf{e}-1\right)+\right.\\
&\left.+\left(\mathbf{e}^{\mathrm{T}}\,\mathbf{b}_2\cdot\mathbf{e}-1\right)\mathbf{b}_3\right)+2\,c^{\mathrm{o}}_{33}\,\mathbf{b}_3^{\mathrm{T}}\left(\mathbf{e}^{\mathrm{T}}\,\mathbf{b}_3\cdot\mathbf{e}-1\right)\Big]\cdot\mathbf{e}\,\mathrm{d}V\,,
\end{aligned} \tag{54}$$

and for $k = 4, 5, 6$:

$$I^{\mathrm{o}}_k = \frac{1}{8}\int_V c^{\mathrm{o}}_{kk}\left[\left(\mathbf{b}_k+\mathbf{b}_k^{\mathrm{T}}\right)\left(\mathbf{e}^{\mathrm{T}}\,\mathbf{b}_k\cdot\mathbf{e}\right)+\left(\mathbf{e}^{\mathrm{T}}\,\mathbf{b}_k\cdot\mathbf{e}\right)\left(\mathbf{b}_k+\mathbf{b}_k^{\mathrm{T}}\right)\right]\cdot\mathbf{e}\,\mathrm{d}V\,. \tag{55}$$

The vector of the orthotropic GEF $\mathbf{Q}^{\mathrm{o}}$ is finally equal to the sum of the orthotropic stiffness integrals (54), (55):

$$\mathbf{Q}^{\mathrm{o}}_{\mathrm{e}} = \sum_{i=1}^{6} I^{\mathrm{o}}_i\,. \tag{56}$$

3.2. Nonlinear Cauchy-elastic orthotropic material

The formulation of the orthotropic GEFs derivation (56) is now extended to a special case of nonlinear orthotropic elasticity. First, the number of independent material parameters c^{N}_{ij} is reduced from 9 to 4. They are then used to

define the following stress-strain relations:

$$\sigma_{\mathrm{P2},11} = c_{11}^{\mathrm{N}} \left(\varepsilon_{11} + D_1\, \varepsilon_{11}^2\right) + c_{12}^{\mathrm{N}} \left(\varepsilon_{22} + \varepsilon_{33}\right) \,, \tag{57}$$

$$\sigma_{\mathrm{P2},22} = c_{22}^{\mathrm{N}} \left(\varepsilon_{22} + D_2\, \varepsilon_{22}^2\right) + c_{12}^{\mathrm{N}} \left(\varepsilon_{11} + \varepsilon_{33}\right) \,, \tag{58}$$

$$\sigma_{\mathrm{P2},33} = c_{22}^{\mathrm{N}}\, \varepsilon_{33} + c_{12}^{\mathrm{N}} \left(\varepsilon_{11} + \varepsilon_{22}\right) \,, \tag{59}$$

$$\sigma_{\mathrm{P2},ij} = c_{44}^{\mathrm{N}}\, \varepsilon_{ij} \,, \quad i,j = 1,2,3, \quad i \neq j \,, \tag{60}$$

with D_k as constants that characterize nonlinear behaviour in normal directions. In this way, the X_1-X_2 in-plane parameters are used to characterize the material in direction X_3. By doing so, a dynamical characterization of a variety of advanced materials, characterized by two-dimensional, full-field measurements [3], is made possible. It should be noted at this point that the used plate element produces zero strains for the arbitrary rigid-body movement, as shown by Mikkola and Shabana in [18]. The presented Cauchy-elastic constitutive law (57)-(60) therefore satisfies the objectivity requirements, since for the rigid-body movement the stresses are also zero.

The elastic properties of the nonlinearly elastic material are strain-dependent. They are obtained as the stress derivatives with respect to the Green–Lagrange strains:

$$c_{ij}^{\mathrm{N}} = \frac{\partial \sigma_{\mathrm{P2},ij}}{\partial \varepsilon_{ij}} \,, \tag{61}$$

and are incorporated into the nonlinear GEFs calculation during the time integration.

The stiffness integrals for the nonlinearly elastic and orthotropic material $I_{\mathrm{N}}^{\mathrm{o}}$ are derived, using the same procedure as in Section 3. For the sake of brevity, only the final form of $I_{\mathrm{N}}^{\mathrm{o}}$ is given here, as:

$$I_{\mathrm{N}}^{\mathrm{o}} = \sum_{i=1}^{6} I_{\mathrm{N}i}^{\mathrm{o}} \,, \tag{62}$$

where the partial stiffness integrals are:

$$\begin{aligned} I_{\mathrm{N1}}^{\mathrm{o}} =& \frac{1}{4} \int_V \Big[\Big(c_{11}\, \mathbf{b}_1^{\mathrm{T}} + c_{12} \left(\mathbf{b}_2^{\mathrm{T}} + \mathbf{b}_3^{\mathrm{T}} \right) \Big) \left(\mathbf{e}^{\mathrm{T}} \mathbf{b}_1 \cdot \mathbf{e} - 1 \right) + \Big(c_{11} \left(\mathbf{e}^{\mathrm{T}} \mathbf{b}_1 \cdot \mathbf{e} - 1 \right) + \\ & + c_{12} \left(\mathbf{e}^{\mathrm{T}} \mathbf{b}_2 \cdot \mathbf{e} + \mathbf{e}^{\mathrm{T}} \mathbf{b}_3 \cdot \mathbf{e} - 2 \right) + \frac{3\, c_{11}\, D_1}{2} \left(\mathbf{e}^{\mathrm{T}} \mathbf{b}_1 \cdot \mathbf{e} - 1 \right)^2 \Big) \mathbf{b}_1 \Big] \cdot \mathbf{e}\, \mathrm{d}V \,, \end{aligned} \tag{63}$$

$$\begin{aligned} I_{\mathrm{N2}}^{\mathrm{o}} =& \frac{1}{4} \int_V \Big[\Big(c_{22}\, \mathbf{b}_2^{\mathrm{T}} + c_{12} \left(\mathbf{b}_1^{\mathrm{T}} + \mathbf{b}_3^{\mathrm{T}} \right) \Big) \left(\mathbf{e}^{\mathrm{T}} \mathbf{b}_2 \cdot \mathbf{e} - 1 \right) + \Big(c_{22} \left(\mathbf{e}^{\mathrm{T}} \mathbf{b}_2 \cdot \mathbf{e} - 1 \right) + \\ & + c_{12} \left(\mathbf{e}^{\mathrm{T}} \mathbf{b}_1 \cdot \mathbf{e} + \mathbf{e}^{\mathrm{T}} \mathbf{b}_3 \cdot \mathbf{e} - 2 \right) + \frac{3\, c_{22}\, D_2}{2} \left(\mathbf{e}^{\mathrm{T}} \mathbf{b}_2 \cdot \mathbf{e} - 1 \right)^2 \Big) \mathbf{b}_2 \Big] \cdot \mathbf{e}\, \mathrm{d}V \,, \end{aligned} \tag{64}$$

$$\begin{aligned} I_{\mathrm{N3}}^{\mathrm{o}} =& \frac{1}{4} \int_V \Big[c_{12}^{\mathrm{o}} \Big(\mathbf{b}_1^{\mathrm{T}} \left(\mathbf{e}^{\mathrm{T}}\, \mathbf{b}_3 \cdot \mathbf{e} - 1 \right) + \left(\mathbf{e}^{\mathrm{T}}\, \mathbf{b}_1 \cdot \mathbf{e} - 1 \right) \mathbf{b}_3 + \mathbf{b}_2^{\mathrm{T}} \left(\mathbf{e}^{\mathrm{T}}\, \mathbf{b}_3 \cdot \mathbf{e} - 1 \right) + \\ & + \left(\mathbf{e}^{\mathrm{T}}\, \mathbf{b}_2 \cdot \mathbf{e} - 1 \right) \mathbf{b}_3 \Big) + 2\, c_{22}^{\mathrm{o}}\, \mathbf{b}_3^{\mathrm{T}} \left(\mathbf{e}^{\mathrm{T}}\, \mathbf{b}_3 \cdot \mathbf{e} - 1 \right) \Big] \cdot \mathbf{e}\, \mathrm{d}V \,, \end{aligned} \tag{65}$$

and $I^{\mathrm{o}}_{\mathrm{N}i}$ for $i = 4, 5, 6$, take the form like (55), with $c_{kk} = c_{44}$.

The integrals (47)-(50), (54)-(55) and (63)-(65) are evaluated numerically [18]. In this research, the three-dimensional *Gaussian quadrature* is employed [5]. It should be noted here that the number of points for integration should be chosen carefully, since it directly affects the computational cost during the time integration.

4. Numerical experiments

Several numerical simulations are studied here to validate the theory and to show the dynamic response of an anisotropic material. All the simulations analyze a thick plate structure of dimensions $1.0 \times 1.0 \times 0.075$ m (Fig. 2). The plate is discretized by 4, 16, 25 or 36 finite elements that are interconnected using the kinematic constraints (20)–(23). All the analyses were performed on a 2.93-GHz processor PC using Matlab®. For the dynamical simulations, the Adams–Bashforth–Moulton "predictor–corrector" method with a variable time step was employed for the time integration. The computational times are reported in Table 3.

4.1. Free vibration test

The purpose of this simulation is to show the free-vibration response of a real, linearly elastic, orthotropic, polyimide material, characterized by 9 independent material parameters. In [8], the 9 independent, compliance-material parameters of a *Kapton E*® polyimide with $\rho = 1366$ kg/m^3, are determined. By using these parameters with (52), the orthotropic elasticity matrix (51) is obtained by inversion, as:

$$\mathbf{E}^{\mathrm{o}} = \begin{bmatrix} 10.44 & 5.824 & 5.908 & 0 & 0 & 0 \\ 5.824 & 9.382 & 5.522 & 0 & 0 & 0 \\ 5.908 & 5.522 & 15.05 & 0 & 0 & 0 \\ 0 & 0 & 0 & 1.970 & 0 & 0 \\ 0 & 0 & 0 & 0 & 0.490 & 0 \\ 0 & 0 & 0 & 0 & 0 & 0.270 \end{bmatrix} \text{GPa} \,, \tag{66}$$

based on which the GEF vector is assembled in the form of (56). The model for the free-vibration analysis is shown in Fig. 2. The impact vector-force $\mathbf{F}(t)$ is applied at the node "Q_2", as:

$$\mathbf{F}(t) = \begin{cases} [0,\, 0,\, -50]^{\mathrm{T}} \text{ kN}\,; & t < 0.0075 \\ \mathbf{0}\,; & 0.0075 \geq t > 0.2\,. \end{cases} \,, \tag{67}$$

for 0.2 s of simulation time.

Fig. 3 shows the undamped response of the plate in comparison to the numerical solution, obtained by *Pro/Mechanica* using 603 linearly elastic tetrahedrons. The solution obtained by only 4 ANCF elements is found to be slightly stiffer in comparison to the standard FE solution. However, the use of a denser ANCF grid improves the convergence.

The eigenvalue analysis was also performed to assess the effects of the higher vibration modes. For the impact excitation (Fig. 2), the Fourier transform was employed to obtain the amplitude-frequency spectrum for the point "Q_2" response. In Fig. 4, a comparison of the spectra is shown for the 36-elements ANCF solution against the standard FE solution. The first 8 natural frequencies are also marked. They were identified using the modal analysis and are

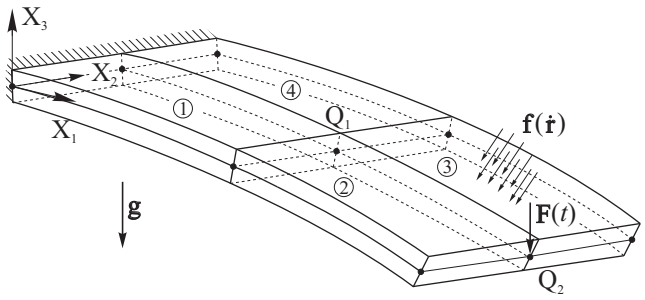

Figure 2: A clamped orthotropic plate; excitation and damping

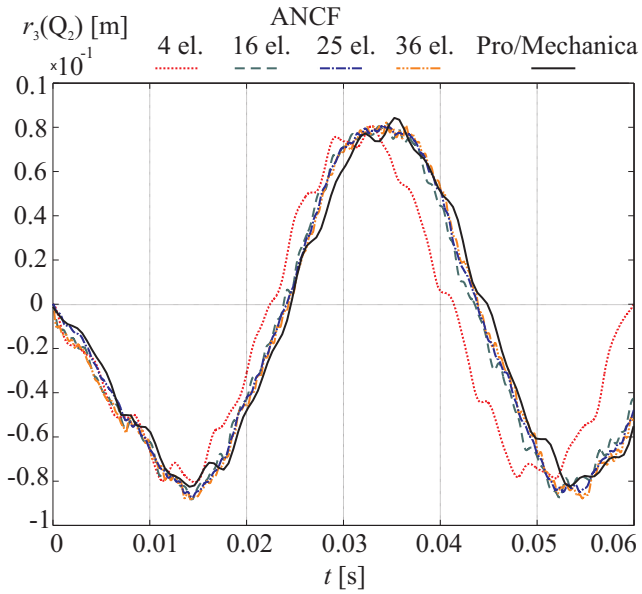

Figure 3: The undamped response of the point "Q_2"

reported in Table 1. In our case, the first mode is dominant and is well captured by the ANCF elements. Further, up to 100 Hz the frequency response is in good agreement with the standard FE solution. However, in the higher-frequency range the (continuum-based) ANCF elements perform poorly, since they are known to suffer from locking effects [24].

When using the formulation of the equation of motion (24, 25), the satisfaction of the kinematic constraints over time needs to be checked. Table 2 shows the accumulated errors at the end of the simulation time. The results are presented for the point Q_1, which connects 4 ANCF elements. The reference values are taken to be those of element "1". The difference of order 10^{-9} or less for all cases is found to be acceptable for our purpose and justifies the used computational procedure.

To simulate a real dynamical problem, the implementation of the gravitational force and the external, nonlinear

Table 1: The natural frequencies of the clamped plate up to 500 Hz, obtained with Pro/Mechanica modal analysis

Mode	1	2	3	4	5	6	7	8	9
Natural frequency [Hz]	24.9	29.2	94.3	198.5	207.7	308.4	315.2	495.0	499.3

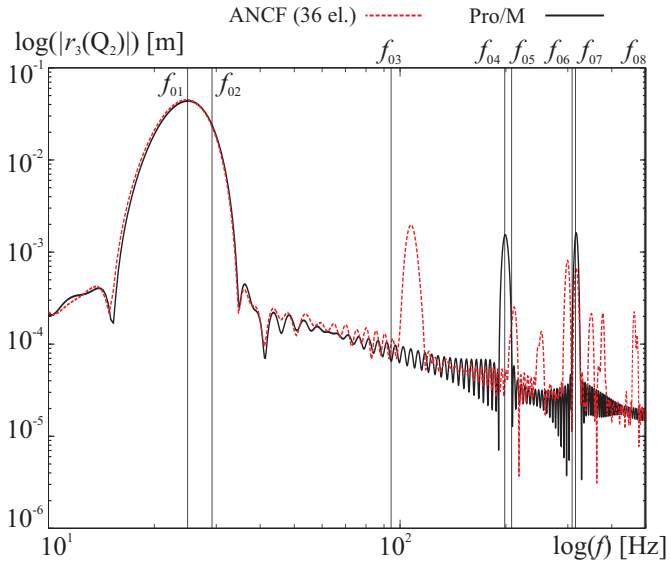

Figure 4: The amplitude-frequency spectrum for the point "Q_2" response

damping force $\mathbf{f}(\dot{\mathbf{r}})$, defined according to Section 2, is also shown for the case of the impact excitation (Fig. 2). The linear and quadratic damping parameters are arbitrarily chosen as $\alpha_1 = 530\ \mathrm{kg \cdot s^{-1} m^{-2}}$ and $\alpha_2 = 3610\ \mathrm{kg \cdot m^{-3}}$. The dynamic response of the plate is shown in Fig. 5, where the global vertical positions r_3 are plotted for the points "Q_1" and "Q_2". Due to the external damping the displacement amplitudes decrease with time. The relatively long computational times (Table 3) are due to the material stiffness and its effect on the integration of (25); in the ANCF, the continuum-based elements are known to exhibit stiff behaviour due to the relatively high material stiffness. For this simulation the 2-point Gaussian quadrature was used.

4.2. Large deformation of a highly flexible material

The aim of the following simulations is to show the static and dynamic responses of the nonlinearly elastic and orthotropic ANCF plate element. Such an element should be able to describe the nonlinear dynamic behaviour of the aforementioned stone-wool fleece; a highly flexible and anisotropic material. The GEF vector (62), characterized by 4 orthotropic material parameters and nonlinearly elastic stress–strain relations (57)-(58), is used for this analysis. Since the real material parameters of the stone-wool fleece are at the present time unknown, orientational values are

Table 2: Satisfaction of kinematic constraints at the end of simulation time $t = 0.2$ at point Q_1 (Fig. 2)

$t = 0.2$ s	$\left(r_1^i - r_1^1\right)$ [m]	$\left(r_2^i - r_2^1\right)$ [m]	$\left(r_3^i - r_3^1\right)$ [m]	$\left(r_{1,x_1}^i - r_{1,x_1}^i\right)$	$\left(r_{2,x_1}^i - r_{2,x_1}^1\right)$	$\left(r_{3,x_1}^i - r_{3,x_1}^1\right)$	
$\mathbf{e}_{Q_1}^2 - \mathbf{e}_{Q_1}^1$	-0.0370	0.1980	0.3700	-1.3050	1.6820	1.4690	
$\mathbf{e}_{Q_1}^3 - \mathbf{e}_{Q_1}^1$	-4.9960	0.0010	0.0020	0.0010	0.0100	0.0300	$\cdot 10^{-9}$
$\mathbf{e}_{Q_1}^4 - \mathbf{e}_{Q_1}^1$	-5.0010	5.0080	0.0850	0.0130	-0.0010	-0.0140	
	$\left(r_{1,x_2}^i - r_{1,x_2}^1\right)$	$\left(r_{2,x_2}^i - r_{2,x_2}^2\right)$	$\left(r_{3,x_2}^i - r_{3,x_2}^1\right)$	$\left(r_{1,x_3}^i - r_{1,x_3}^1\right)$	$\left(r_{2,x_3}^i - r_{2,x_3}^1\right)$	$\left(r_{3,x_3}^i - r_{3,x_3}^1\right)$	
$\mathbf{e}_{Q_1}^2 - \mathbf{e}_{Q_1}^1$	-2.2690	-5.9450	5.4070	-0.2020	-4.8700	-1.4340	
$\mathbf{e}_{Q_1}^3 - \mathbf{e}_{Q_1}^1$	-0.0040	-0.0040	0.0130	-0.1260	-0.0160	0.0010	$\cdot 10^{-9}$
$\mathbf{e}_{Q_1}^4 - \mathbf{e}_{Q_1}^1$	0.0000	-0.0050	0.2350	0.0170	-0.2410	-0.0020	

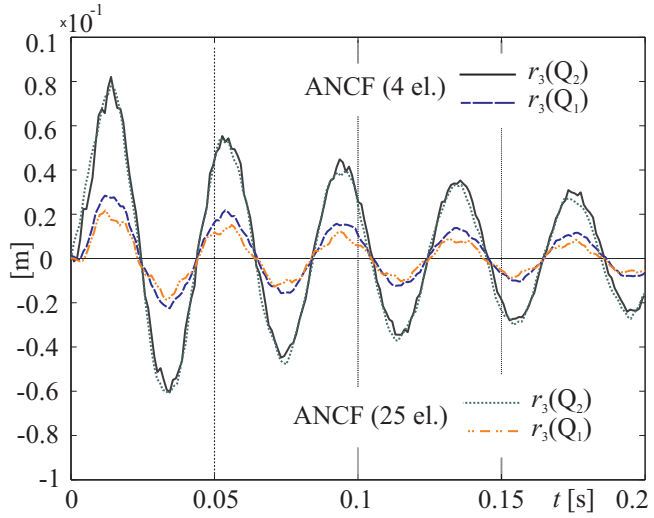

Figure 5: Vertical displacement of points "Q_1" and "Q_2" during damped free vibration

used that roughly approach the real ones:

$$\begin{aligned} &c_{11} = 30.4 \cdot 10^4 \text{ Pa}\,, \quad c_{12} = 5.26 \cdot 10^4 \text{ Pa}\,, \quad c_{22} = 9.41 \cdot 10^4 \text{ Pa}\,, \\ &c_{44} = 0.52 \cdot 10^4 \text{ Pa}\,, \quad c_{33} = c_{22}\,, \quad c_{55} = c_{66} = c_{44}, \quad c_{13} = c_{23} = c_{12}\,. \end{aligned} \tag{68}$$

4.2.1. Static analysis

The static test consists of a simply supported plate with a vertical force applied at the middle surface node Q_3 (Fig. 6). The accelerations and velocities vanish from the formulation, thereby defining the static equilibrium that is solved for nodal coordinates employing the Newton-Raphson procedure. The validation of the presented element is performed with the comparison against the linear solution, obtained with Pro/M. To induce small deformation, the force is defined as $\mathbf{F}_s = 1$ N. For a small deformation the ANCF solution should approach the commercial solution when using small values for the nonlinearity parameters $D_1 = D_2 = 10^{-5}$; the contribution of the quadratic strain terms (57)-(58) is thereby neglected.

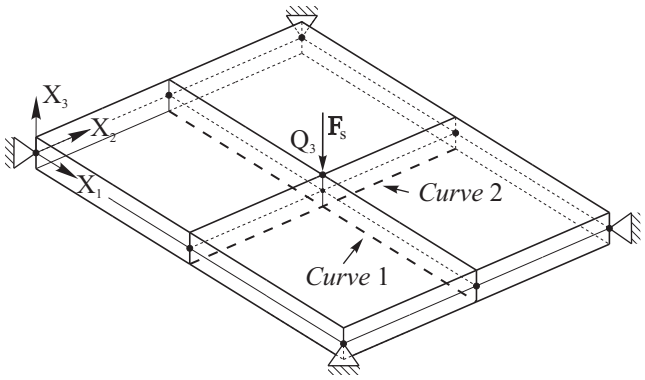

Figure 6: Simply supported nonlinearly elastic plate for static analysis

In Figs. 7 and 8, the comparison of the vertical deflections is shown for the two surface curves (Fig. 6). The Pro/M solution is obtained using 472 linearly elastic and orthotropic elements. In this case, small number of ANCF elements is unable to adequately describe the localized middle-plate deflection; however, an increased number of elements is observed to approach the standard FE solution. The orthotropic response is also clearly visible; due to the different stiffnesses in X_1 direction, the deflections towards the ends of *curve* 1 is also different in comparison to those of *curve* 2.

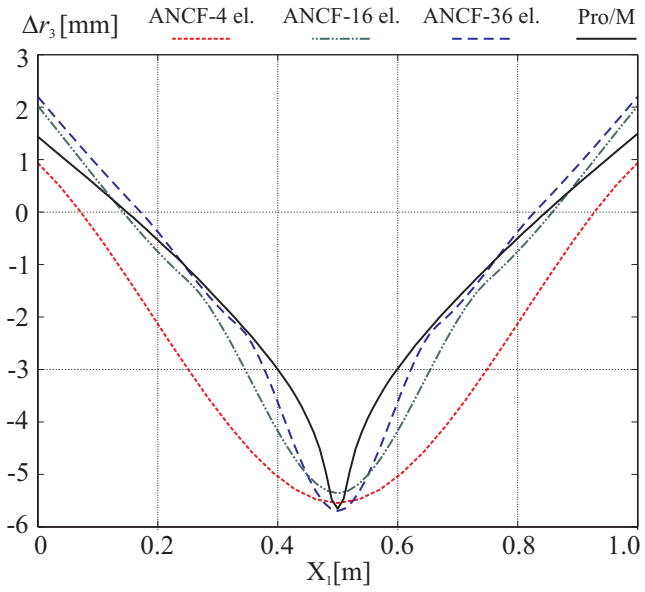

Figure 7: Vertical deflection Δr_3 across the plate for *curve* 1 (Fig. 6)

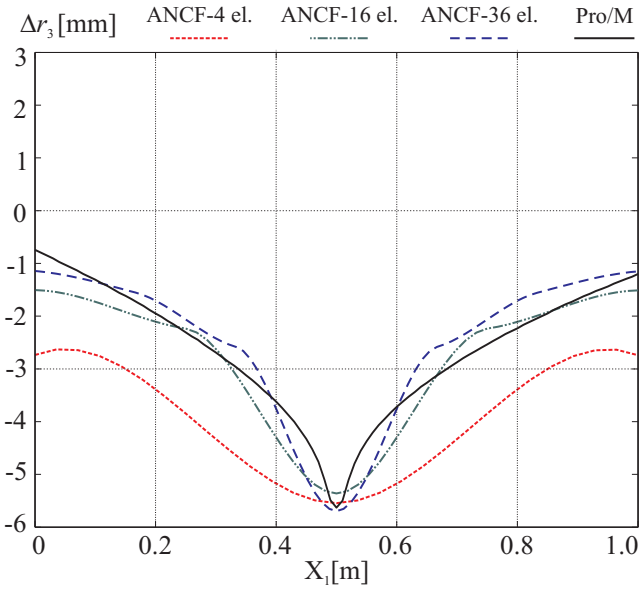

Figure 8: Vertical deflection Δr_3 across the plate for *curve* 2 (Fig. 6)

4.2.2. Large-deformation dynamical system

An example of nonlinear dynamic analysis is presented in the following using the element from Section 3.2. Fig. 9 shows the setup for a large-deformation simulation of a thick clamped plate that vibrates under the gravity and the two time-dependent external forces $\mathbf{F}(t) = 750\,t/\mathrm{s}$ N. The external forces are applied symmetrically at the end-nodes in the direction $\alpha = \beta = 45^\circ$ and $\gamma = 10^\circ$ with respect to the inertial frame axes.

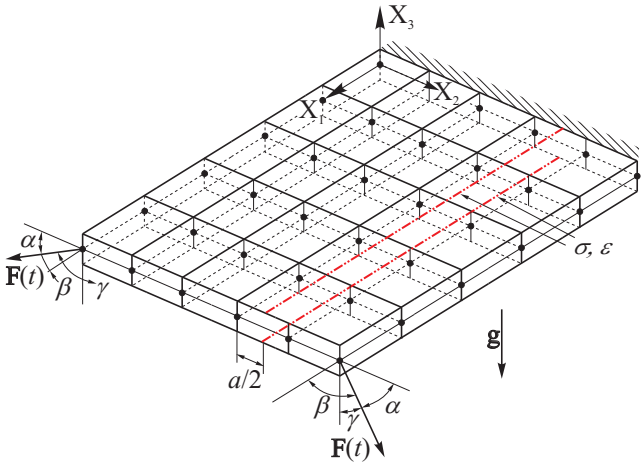

Figure 9: A large-deformation test for a nonlinearly elastic and orthotropic material, characterized by 4 material parameters

A total of 25 ANCF elements are used for the 1 s simulation time. The nonlinearity parameters are $D_1 = 0.02$ and $D_2 = 0.09$. After 0.5 s and 1 s, the configurations of the plate are shown in Fig. 10, from which the large displacements and strains are evident. To analyze the final configuration, the Cauchy stresses were calculated from 2$^{\text{nd}}$ Piola-Kirchhoff stresses as $\boldsymbol{\sigma} = |J|^{-1}\mathbf{J}\,\boldsymbol{\sigma}_{\text{P2}}\,\mathbf{J}^{\text{T}}$. In Figs. 11 and 12, the interpolated normal Cauchy stresses σ_{11} and σ_{22}, and normal Green–Lagrange strains ε_{11} and ε_{22}, are shown for the upper and lower surface curves across the plate (Fig. 9). The strains and stresses are both highly nonlinear, yet they confirm the expected response; the plate stretch prevails in the X_1 direction due to the own dead weight and is higher in the lower-surface curve. The stresses σ_{11} towards the plate's free end are also higher in comparison to σ_{22} due to the higher stiffness in direction X_1. The stresses and strains are both continuous across the elements' nodes; however, they are discontinuous between the elements' surfaces. In Figs. 11 and 12, average values at elements' interfaces are calculated, based on which the curves are fitted across the plate.

Due to the relatively low overall material stiffness, the computational time is considerably less than for the previous simulations (Table 3). The 3-point Gaussian quadrature was used in this case for the evaluation of the stiffness integrals.

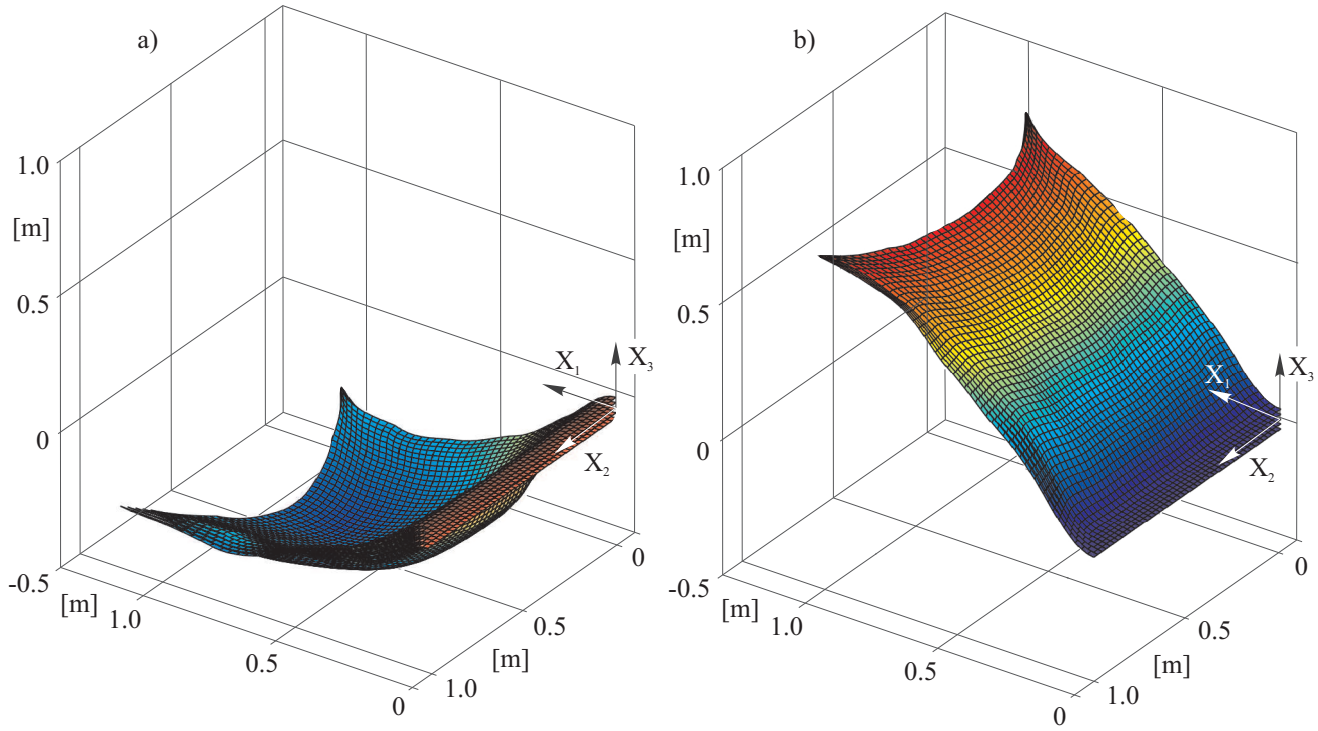

Figure 10: The configuration of the orthotropic clamped plate under the external vector-force loading after: a) 0.5 s and b) 1 s

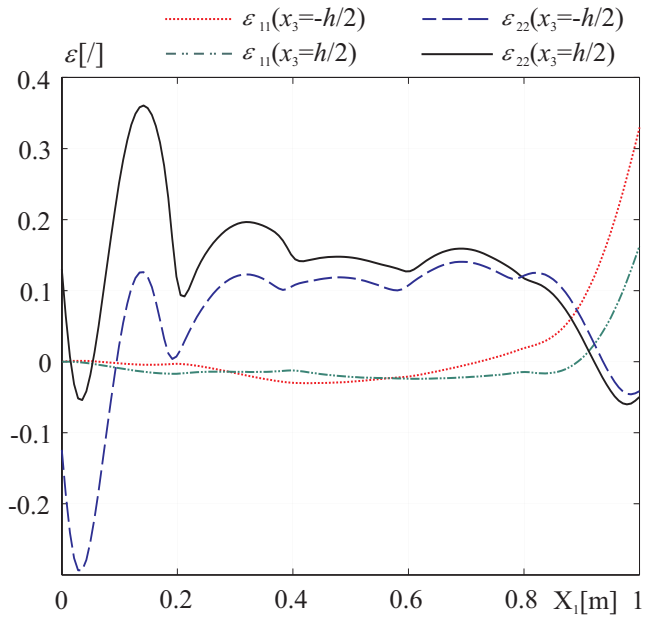

Figure 11: The Green–Lagrange strains on the surface curves (Fig. 9), after 0.5 s

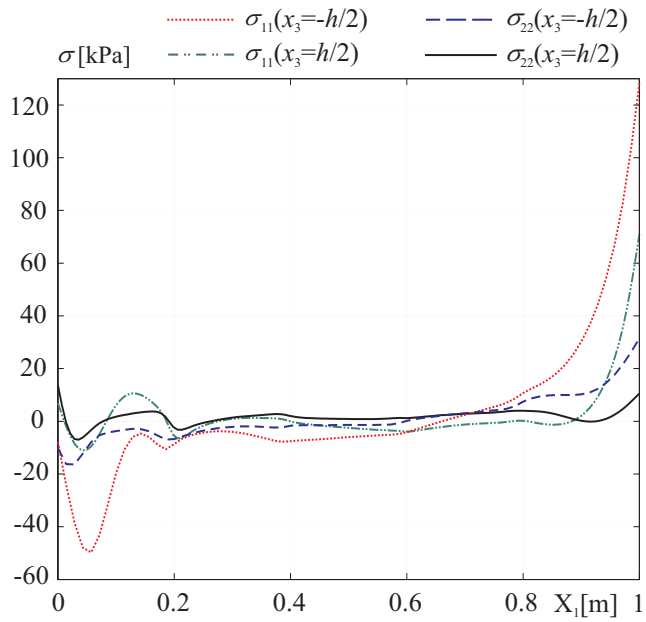

Figure 12: The normal Cauchy stresses on the surface curves (Fig. 9), after 0.5 s

Table 3: Computational times for all numerical examples

	Linear orthotropy (Free vibration)		Nonlinear orthotropy	
	undamped	damped	static	dynamic
4 elements	1.1 h	2.7 h	0.4 min	/
16 elements	5.1 h	8.3 h	4.0 min	13.8 min
25 elements	7.1 h	11.2 h	6.0 min	34.4 min
36 elements	10.9 h	23.2 h	17.5 min	49.2 min

5. Conclusion

In this research, an implementation of the material anisotropy into the absolute nodal coordinate formulation (ANCF) is investigated in terms of the generalized elastic forces (GEFs) of the elastic and homogeneous material using the continuum-based, thick ANCF plate elements. To address the anisotropy, the derivation procedure of the element's GEF vector is presented for the most general case of a fully anisotropic material, characterized by 21 independent material parameters. By systematically reducing the number of independent coefficients in the elasticity matrix, the same procedure is used to define two GEF vectors for materials of lower-order anisotropy. Specifically, a GEF vector for a linearly elastic, orthotropic material, characterized by 9 independent parameters is given first, and then further extended to the special case of a nonlinear, Cauchy-elastic orthotropic material. For the latter case, the material is characterized by the 4 independent in-plane material parameters.

The theory validation and the anisotropic effects are presented with numerical simulations. The displacement and eigenfrequency analyses are performed for the free-vibration test of the clamped plate, made of a real, linearly elastic and orthotropic polyimide material. The convergence and satisfaction of the kinematic constraints over time are also studied for this case. The static and dynamic analyses of a highly flexible, Cauchy-elastic and orthotropic material are also performed. To observe the anisotropic responses, the convergence and results of these simulations are presented in terms of the displacements, stresses and strains.

6. Appendix

The element shape-function matrix $\mathbf{S}$ is defined as:

$$\mathbf{S} = [S_1\,\mathbf{I},\ \ S_2\,\mathbf{I},\ \ \ldots,\ \ S_{16}\,\mathbf{I}]\ , \tag{69}$$

where $\mathbf{I}$ is a 3×3 identity matrix, and:

$$
\begin{aligned}
S_1 &= -(\xi-1)(\eta-1)(2\eta^2-\eta+2\xi^2-\xi-1)\,,\\
S_2 &= -a\,\xi(\xi-1)^2(\eta-1)\,,\\
S_3 &= -b\,\eta(\eta-1)^2(\xi-1)\,,\\
S_4 &= h\,\zeta(\xi-1)(\eta-1)\,,\\
S_5 &= \xi(2\eta^2-\eta-3\xi+2\xi^2)(\eta-1)\,,\\
S_6 &= -a\,\xi^2(\xi-1)(\eta-1)\,,\\
S_7 &= b\,\xi\,\eta(\eta-1)^2\,,\\
S_8 &= -h\,\xi\,\zeta(\eta-1)\,,\\
S_9 &= -\xi\,\eta(1-3\xi-3\eta+2\eta^2+2\xi^2)\,,\\
S_{10} &= a\,\xi^2\,\eta(\xi-1)\,,\\
S_{11} &= b\,\xi\,\eta^2(\eta-1)\,,\\
S_{12} &= h\,\zeta\,\xi\eta\,,\\
S_{13} &= \eta(\xi-1)(2\xi^2-\xi-3\eta+2\eta^2)\,,\\
S_{14} &= a\,\xi\,\eta(\xi-1)^2\,,\\
S_{15} &= -a\,\eta^2(\xi-1)(\eta-1)\,,\\
S_{16} &= -h\,\eta\,\zeta(\xi-1)\,, \quad \xi = x_1/a,\ \eta = x_2/b\,, \zeta = x_3/h\,,
\end{aligned}
$$

where a, b and h are the length, width and height of the element, respectively. The presented shape function $\mathbf{S}$ ensures positions and position-vector gradients' continuity at the nodal points; however, it does not ensure the gradients' continuity at the element's interface.

7. Acknowledgments

The operation was partially financed by the European Union, European Social Fund.

[1] Abbas, L. K., Rui, X., Hammoudi, Z. S.: Plate/shell element of variable thickness based on the absolute nodal coordinate formulation. Nonlinear Dynamics **224**, 127–141 (2010)

[2] Abbas, L., Rui, X., Marzocca, P.: Panel flutter analysis of plate element based on the absolute nodal coordinate formulation. Multibody System Dynamics **27**, 135–152 (2012)

[3] Avril, S., Bonnet, M., Bretelle, A., Grdiac, M., Hild, F., Ienny, P., Latourte, F., Lemosse, D., Pagano, S., Pagnacco, E., Pierron, F.: Overview of Identification Methods of Mechanical Parameters Based on Full-field Measurements. Experimental Mechanics **48**, 381–402 (2008)

[4] Bronstein, I.N., Semendyayev, M.G.: Handbook of Mathematics, Fourth Edition. Springer-Verlag (2003)

[5] Burden, R.L., Faires, D.J.: Numerical Analysis, 9 edn. Brooks Cole (2010)

[6] Čepon, G., Boltežar, M.: Dynamics of a belt-drive system using a linear complementarity problem for the belt-pulley contact description. Journal of Sound and Vibration **319**(3-5), 1019–1035 (2009)

[7] Čepon, G., Manin, L., Boltežar, M.: Introduction of damping into the flexible multibody belt-drive model: A numerical and experimental investigation. Journal of Sound and Vibration **324**(1-2), 283–296 (2009)

[8] Cho, S.H., Kim, G., McCarthy, T.J., Farris, R.J.: Orthotropic elastic constants for polyimide film. Polymer Engineering & Science **41**(2), 301–307 (2001)

[9] Dmitrochenko, O.: Finite elements using absolute nodal coordinates for large-deformation flexible multibody dynamics. Journal of Computational and Applied Mathematics **215**(2), 368–377 (2008)

[10] Dmitrochenko, O., Mikkola, A.: A formal procedure and invariants of a transition fromconventional finite elements to the absolute nodal coordinate formulation. Multibody System Dynamics **22**, 323–339 (2009)

[11] Dufva, K., Kerkkänen, K., Maqueda, L.G., Shabana, A.A.: Nonlinear dynamics of three-dimensional belt drives using the finite-element method. Nonlinear Dynamics **48**(4), 449–466 (2007)

[12] Hussein, B., Negrut, D., Shabana, A.A.: Implicit and explicit integration in the solution of the absolute nodal coordinate differential/algebraic equations. Nonlinear Dynamics **54**, 283–296 (2008)

[13] Kerkkänen, K., GarcaVallejo, D., Mikkola, A.: Modeling of belt-drives using a large deformation finite element formulation. Nonlinear Dynamics **43**, 239–256 (2006)

[14] Langerholc, M., Česnik, M., Slavič, J., Boltežar, M.: Experimental validation of a complex, large-scale, rigid-body mechanism. Engineering Structures **36**, 220–227 (2012)

[15] Langerholc, M., Slavič, J., Boltežar, M.: Absolute nodal coordinates in digital image correlation. Experimental Mechanics, DOI:I:10.1007/s11340-012-9691-4, (2012)

[16] Maqueda, L.G., Mohamed, A.N.A., Shabana, A.A.: Use of general nonlinear material models in beam problems: Application to belts and rubber chains. Journal of Computational and Nonlinear Dynamics **5**(2), 021,003 (2010)

[17] Maqueda, L.G., Shabana, A.A.: Poisson modes and general nonlinear constitutive models in the large displacement analysis of beams. Multibody system dynamics **18**(3), 375–396 (2007)

[18] Mikkola, A., Shabana, A.A.: A non-incremental finite element procedure for the analysis of large deformation of plates and shells in mechanical system applications. Multibody System Dynamics **9**, 283–309 (2003)

[19] Nada, A., El-Assal, A.: Absolute nodal coordinate formulation of large-deformation piezoelectric laminated plates. Nonlinear Dynamics **67**, 2441–2454 (2012)

[20] Newnham, R.E.: Properties Of Materials: Anisotropy, Symmetry, Structure. Oxford University Press (2005)

[21] Pogorelov, D., Dmitrochenko, O.: Generalization of plate finite elements for absolute nodal coordinate formulation. Multibody System Dynamics **10**(1), 17–43 (2003)

[22] Shabana, A.A.: Computational Dynamics, Third Edition. John Wiley & Sons Ltd (2010)

[23] Shabana, A.A.: Computational Continuum Mechanics. Cambridge University Press (2008)

[24] Schwab, A.L., Gerstmayr, J., Meijaard, J. P.: Comparison of three-dimensional flexible thin plate elements for multibody dynamic analysis: finite element formulation and absolute nodal coordinate formulation. ASME Conference Proceedings **4806X**, 1059–1070 (2007)

[25] Sugiyama, H., Shabana, A.A.: Application of plasticity theory and absolute nodal coordinate formulation to flexible multibody system dynamics. Journal of mechanical design **126**(3), 478–487 (2004)

[26] Sugiyama, H., Shabana, A.A.: On the use of implicit integration methods and the absolute nodal coordinate formulation in the analysis of elasto-plastic deformation problems. Nonlinear Dynamics **37**, 245–270 (2004)

[27] Tian, Q., Liu, C., Machado, M., Flores, P.: A new model for dry and lubricated cylindrical joints with clearance in spatial flexible multibody systems. Nonlinear Dynamics **64**, 25–47 (2011)

[28] Yoo, P.S., Pogorelov, D., Dmitrochenko, O.: Large deflection analysis of a thin plate: Computer simulations and experiments. Multibody System Dynamics **11**, 185–208 (2004)

[29] Yu, L., Ren, G.T.: Integration of absolute nodal elements into multibody system. Nonlinear Dynamics **62**, 931–943 (2010)